Potential accuracies of some new approaches for determination by Thomson scattering lidar of the electron temperature profiles in thermonuclear plasmas

Ljuan L. Gurdev*, Tanja N. Dreischuh, Dimitar V. Stoyanov
Institute of Electronics, Bulgarian Academy of Sciences, 72 Tzarigradsko shosse, Sofia, Bulgaria

ABSTRACT

Two new approaches are proposed for determination by Thomson scattering lidar of the electron temperature in thermonuclear fusion plasmas. They are based on an analysis of the relativistic Thomson scattering spectrum. One of them is based on the unambiguous temperature dependence of the ratio of the return-signal powers of two spectral regions. The second approach is based on the unambiguous temperature dependence of the "center-of-mass wavelength" of the lidar-return spectrum. Analytical expressions are derived of the corresponding errors in the determination of the electron temperature. Their validity is confirmed by computer simulations. On the basis of the theoretical expressions a comparison is performed between the potential accuracies of the new methods and the routine fitting approach. As a result it is shown that the new approaches would have comparable efficiency with the fitting approach. Thus the three (the fitting and the novel) approaches may be used for mutually validating the results obtained for the electron temperature. They may be used as well for distinguishing the real inhomogeneities in the recovered temperature profiles from apparent ones due to statistical fluctuations. The novel approaches may also have some practical advantages consisting of the simple, clear and stable measurement procedure without any hypotheses or other considerations about the weight or the variance of the experimental data or the goodness of the fit.

Keywords: Thomson scattering lidar, fusion plasma diagnostics, electron temperature profiles

1. INTRODUCTION

As is well known, the realization of controllable nuclear fusion would ensure the access of human civilization to a practically inexhaustible source of energy. Therefore extreme investigatory and financial efforts have been made for solving this crucial-to-humanity task. Among the nuclear fusion systems developed so far with magnetic or inertial plasma confinement, the Tokamak systems of the former type appear to be the most promising ones. In the recent years, just in the Tokamak-type fusion reactor JET one realized deuteron-triton fusion during 3s, at a maximum produced energy of 21 MJ, mean power of 16.1 MW, and output-to-input power ratio of the order of 0.65.

Effective observation and control of the fusion process is possible only on the basis of effective plasma diagnostics involving the determination with high accuracy and (spatio-temporal) resolution of the electron temperature T_e and concentration n_e in the reactive zone. Because of the high characteristic temperatures [~ $(1\text{-}4)\times10^8$ K] and pressures [~$2.76\text{-}11.04\times10^5$ Pa] in this case, the only effective methods for diagnostics turn out to be the contactless, passive and active optical or microwave ones. Among these, the Thomson-scattering-based lidar-type methods are especially appropriate for simultaneous determination of electron temperature and concentration profiles in fusion plasmas. The approach having been used so far for electron temperature and pressure measurement is based on log-linear or non-linear fit of the experimentally-obtained, relativistically-thermally-broadened lidar-return spectra to the corresponding theoretical expression.

Except the fitting approach, one may develop some new complimentary approaches for determination of the electron temperature and concentration on the basis of an analysis of the relativistic Thomson scattering (TS) spectrum. We propose here two such approaches for measuring the electron temperature. One of them is based on the unambiguous temperature dependence of the ratio of the return-signal powers of two spectral regions. The second approach is based on the unambiguous temperature dependence of the "center-of-mass wavelength" of the lidar-return spectrum. The

* lugurdev@ie.bas.bg; phone 359-2-9795906; fax 359-2-9753201; ie-bas.dir.bg

15th International School on Quantum Electronics: Laser Physics and Applications, edited by Tanja Dreischuh
Elena Taskova, Ekaterina Borisova, Alexander Serafetinides, Proceedings of SPIE Vol. 7027, 702711
 · doi: 10.1117/12.822512

significance of the development of different approaches is that they would mutually validate the results obtained for T_e. Moreover, the use of several independent measurement approaches could help to distinguish the real inhomogeneities in the recovered temperature profiles from seeming ones due to statistical fluctuations. Therefore, the main purpose of our investigations described here is to estimate analytically and by simulations and to compare the potential temperature-measurement accuracies of the three above-mentioned approaches. For this purpose analytical expressions have been derived for the corresponding relative errors in the determination of the electron temperature. Also, the validity of the expressions derived has been confirmed by computer simulations. The comparative numerical analysis of these expressions shows that after an optimization the new approaches would have comparable efficiency with the fitting approach at temperatures $T_e > 1$ keV. Some practical advantages of the novel approaches consist in the simple, clear and stable measurement procedures without special assumptions about the weight or the variance of the experimental data or considerations about the goodness of the fit.

In the following Section 2 we describe the TS lidar return signal from fusion plasmas and the relevant plasma light background. The noise effects are also briefly discussed there. The new approaches proposed for measuring the electron temperature are described in Section 3. Then, the accuracy is analyzed theoretically of all the T_e-measurement approaches (the fitting approach and the new ones). In Section 4, the results from Monte Carlo simulations are described that verify the expressions obtained theoretically for the corresponding errors in the determination of T_e. Also, on the basis of the theoretical expressions, the potential accuracies (efficiencies) of the different approaches are numerically compared and discussed. The main results and conclusions from the investigations are summarized in Section 5.

2. LIDAR SIGNAL AND ACCOMPANYING NOISE

In this section we consider and describe the TS lidar return signal in the terms of the lidar practice and theory.

2.1 Lidar equation

The single-scattering lidar equation is the main instrument for quantitative analysis of the Thomson scattering lidar profiles. It describes the relation between the measured lidar profile (the time-to-range resolved profile of the received backscattered light power), the parameters of the lidar system, and the characteristics of the investigated medium (high-temperature plasma) along the lidar line of sight (LOS). When the effective pulse response shape of the lidar (which is a convolution of the sensing laser pulse shape and the pulse response function of the receiving electronics) is shorter than the least longitudinal variation scale of the characteristics of the fusion plasma the short-pulse (δ-pulse) lidar equation is in power. The spectral form of the short-pulse lidar equation is:

$$P[\lambda_s;t(z)]d\lambda_s = K(\lambda_i,\lambda_s)\frac{E_0(\lambda_i)c}{2}\frac{A}{z^2}\eta(\lambda_s,z)\beta[\lambda_i;\lambda_s;n_e(z),T_e(z)]\exp\left\{-\int_0^z[\alpha(\lambda_i,z')+\alpha(\lambda_s,z')]dz'\right\}d\lambda_s, \quad (1)$$

where $P[\lambda_s;t(z)]$ is the mean lidar return signal that is proportional to the backscattered (at angle π) light power received at the moment $t=t(z)$ after the pulse emission and z is the LOS coordinate (distance) of the corresponding scattering volume with respect say to the receiving aperture plane; $t(z)$ is unambiguous linear function of z that may have, e.g., the form $t=(2z-R)/c$, where R is the LOS coordinate of the "point of emitting" the laser pulse at a reference initial moment $t=0$; λ_i and λ_s are respectively the wavelengths of the incident and the backscattered radiation; $K(\lambda_i,\lambda_s)=K_t(\lambda_i)K_t(\lambda_s)K_f(\lambda_s)K_q(\lambda_s)$, $K_t(\lambda_i)$, $K_t(\lambda_s)$, $K_f(\lambda_s)$ and $K_q(\lambda_s)$ are respectively the wavelength-dependent optical transmittance of the plasma-irradiating path, the optical transmittance of the scattered-light collecting path, the receiver filter spectral characteristic, and the quantum efficiency of the photon detection; $E_0(\lambda_i)$ is the incident pulse energy; A is the receiving aperture area; $\eta(\lambda_s,z)$ is the lidar receiving efficiency including in general the vignetting effect; c is the speed of light; $\beta[\lambda_i;\lambda_s;n_e(z),T_e(z)]$ is the Thomson backscattering coefficient normalized by λ_i, at a distance z and a wavelength λ_s, that is given (according to Mattioli[1]) by the expression

$$\beta[\lambda_i;\lambda_s;n_e(z),T_e(z)] = \frac{n_e(z)r_0^2}{\sqrt{\pi}\lambda_i}\frac{c}{v_{th}(z)}\left(1+\frac{15}{16}\frac{v_{th}^2(z)}{c^2}+\frac{105}{512}\frac{v_{th}^4(z)}{c^4}\right)^{-1}\frac{(\lambda_i/\lambda_s)^4}{(1+\lambda_i/\lambda_s)} \times \exp\left\{-\frac{c^2}{v_{th}^2(z)}\left[(\lambda_i/\lambda_s)^{1/2}+(\lambda_s/\lambda_i)^{1/2}-2\right]\right\}, \quad (2)$$

r_o is the classical electron radius, $n_e(z)$ is the electron concentration profile along the LOS, $v_{th}(z) = [2k_B T_e(z)/m_e]^{1/2}$ is the mean thermal velocity of the electrons, $T_e(z)$ is the electron temperature profile along the LOS, m_e is the electron rest mass, k_B is the Boltzmann constant, and $\alpha(\lambda_i,z)$ and $\alpha(\lambda_s,z)$ are respectively the extinction coefficients for λ_i and λ_s at a current distance z. Let us note that practically $\exp\left\{-\int_0^z [\alpha(\lambda_i,z') + \alpha(\lambda_s,z')]dz'\right\} = 1$. Note as well that there are some more accurate expressions of $\beta[\lambda_i;\lambda_s;\ n_e(z),T_e(z)]$ (see e.g.[2]) than that given by Eq.(2). However, the difference in the results obtained for β is small (< 3.8 % for T_e<6 keV). Therefore we shall use the simpler and more compact Eq.(2) for a preliminary estimation and a comparison of the statistical and systematic errors in the determination of T_e by different approaches. For completeness, a comparison between the expression for β of Mattioli[1] [Eq.(2)] and that of Naito et al.[2] is given in Appendix A.

In Eq.(1) one may write that $P = Nh\nu_s$ and $E_0 = N_0 h\nu_i$, where $N = N[\lambda_s;t(z)]$ is the photon detection rate, N_0 is the number of photons in the sensing laser pulse, h is the Planck constant, and $\nu_{s,i} = c/\lambda_{s,i}$. Then, the short-pulse lidar equation describing the photon detection rate for the spectral interval $[\lambda_s,\ \lambda_s + d\lambda_s]$ has the form

$$N[\lambda_s;t(z)]d\lambda_s = K_n(\lambda_i,\lambda_s)\frac{N_0(\lambda_i)c}{2}\frac{A}{z^2}\eta(\lambda_s,z)\beta[\lambda_i;\lambda_s;n_e(z),T_e(z)]d\lambda_s\ , \tag{3}$$

where $K_n(\lambda_i,\lambda_s) = K(\lambda_i,\lambda_s)(\nu_i/\nu_s) = K(\lambda_i,\lambda_s)(\lambda_s/\lambda_i)$. For the photon detection rate for a spectral interval $[\lambda_{s1},\lambda_{s2}]$ we may write

$$N[\lambda_{s1},\lambda_{s2},t(z)] = \frac{N_0 c}{2}\frac{A}{z^2}\int_{\lambda_{s1}}^{\lambda_{s2}} d\lambda_s K_n(\lambda_i,\lambda_s)\eta(\lambda_s,z)\beta[\lambda_i;\lambda_s;n_e(z),T_e(z)]\ . \tag{4}$$

Eq.(2) may also be written in the form

$$\beta[\lambda_i;\lambda_s;n_e(z),T_e(z)] = \beta(z)\xi_1[\lambda_i,v_{th}(z)]\xi_2[\lambda_i,\lambda_s,v_{th}(z)]\ , \tag{5}$$

where we have used the substitutions $\beta(z) = r_0^2 n_e(z)$, $\xi_1[\lambda_i;v_{th}(z)] = \frac{c}{\sqrt{\pi}\lambda_i v_{th}(z)}\left(1 + \frac{15}{16}\frac{v_{th}^2(z)}{c^2} + \frac{105}{512}\frac{v_{th}^4(z)}{c^4}\right)^{-1}$, and $\xi_2[\lambda_i;\lambda_s;v_{th}(z)] = \frac{(\lambda_i/\lambda_s)^4}{(1+\lambda_i/\lambda_s)}\exp\left\{-\frac{c^2}{v_{th}^2(z)}\left[(\lambda_i/\lambda_s)^{1/2} + (\lambda_s/\lambda_i)^{1/2} - 2\right]\right\}$. Then, if we consider M spectral channels, for each of them Eq.(4) could be written as

$$N[\lambda_{s1k},\lambda_{s2k},t(z)] = \frac{N_0 c}{2}\frac{A}{z^2}\beta(z)\xi_1[\lambda_i,v_{th}(z)]\int_{\lambda_{s1k}}^{\lambda_{s2k}} K_n(\lambda_i,\lambda_s)\eta(\lambda_s,z)\xi_2[\lambda_i,\lambda_s,v_{th}(z)]d\lambda_s\ ,\ k=1,...,M\ . \tag{6}$$

The quantity $Q(z) = \frac{N_0 c}{2}\frac{A}{z^2}\beta(z)\xi_1[\lambda_i,v_{th}(z)]\int_0^\infty K_n(\lambda_i,\lambda_s)\eta(\lambda_s,z)\xi_2[\lambda_i,\lambda_s,v_{th}(z)]d\lambda_s$ is equal to the total photon detection rate over the whole spectral range.

Let us write at last for completeness the "long-pulse" lidar equation that is valid at arbitrarily long effective pulse-response shape of the lidar with respect to the characteristic spatial variation scales in plasma. It has the form:

$$P[\lambda_s;t(z)]d\lambda_s = K(\lambda_i,\lambda_s)E_o(\lambda_i)Ad\lambda_s\int_0^z dz' f[2(z-z')/c]\eta(\lambda_s,z')\beta[\lambda_i;\lambda_s;n_e(z'),T_e(z')]z'^{-2}\ , \tag{7}$$

where $f(\theta)$ [s^{-1}] is the effective pulse response function. For a spectral interval $[\lambda_{s1},\lambda_{s2}]$ with central wavelength $\lambda_o = (\lambda_{s1}+\lambda_{s2})/2$, on the basis of Eq.(7) we obtain the following expression of the detected signal power

$$P[\lambda_{s1},\lambda_{s2};t(z)] = E_0(\lambda_i)A\int_0^z dz' f[2(z-z')/c]z'^{-2}\int_{\lambda_{s1}}^{\lambda_{s2}} d\lambda_s K(\lambda_i,\lambda_s)\eta(\lambda_s,z')\beta[\lambda_i;\lambda_s;n_e(z'),T_e(z')] \ . \quad (8)$$

As it is mentioned above, the effective pulse response shape of the lidar is a convolution of the sensing laser pulse shape and the pulse response function of the receiving electronics. In turn, the latter is a convolution of the pulse response shape of the photon detector and that of the digitizer. For estimating the duration τ (and, respectively, the length $c\tau$) of the effective pulse response it is expedient to approximate each of the aforementioned shapes by Gaussian functions (e.g.[3,4]). Then the expression for τ will be $\tau = (\tau_p^2 + \tau_{de}^2 + \tau_{di}^2)^{1/2}$, where τ_p, τ_{de}, and τ_{di} are respectively the durations of the laser pulse, the detector response shape, and the digitizer response shape.

2.2 Plasma light background

The plasma light spectrum consists in general of line and continuum components[4-9]. The line components are due to bound-bound electron transitions in atoms and ions and to electron cyclotron emission in magnetic plasma. The continuum components are due to recombination (free-bound electron transitions) and bremsstrahlung resulting mainly from electron-ion collisions. Waves or other modes of collective motion of charged particles are also a source of plasma emission. In pure fusion plasma the thermal electron energy (> 1keV) essentially exceeds the ionization potential of the hydrogen atom (13.6 eV). Therefore, in the visible wavelength range the radiation due to bound-bound and free-bound electron transitions is feeble and negligible as compared with the bremsstrahlung of electrons in the Coulomb field of deuterium and tritium nuclei. The presence of heavy-element impurities in the fusion plasma leads to the appearance of line radiation component in the visible range. However, the impact of this component is smaller than that of the bremsstrahlung[9]. Note as well that the cyclotron emission spectrum as well as that of the collective-motion-due emission occupy the wavelength region above the far infrared. Thus, it turns out that bremsstrahlung is the dominating component of the fusion plasma light in the visible sprectral range.

The bremsstrahlung photon emissivity spectrum from fusion plasma per unit solid angle is described quantitatively by the expression (see e.g. [6,9])

$$\frac{dE}{d\Omega} = 7.56\times10^{-21} Z_{\text{eff}} \lambda^{-1} (k_B T_e)^{-1/2} n_e n_i \exp\left(-\frac{hc}{\lambda k_B T_e}\right)\tilde{g}_{ff}(\lambda, T_e) \qquad \left[\frac{\text{photons}}{\text{m}^4 s}\right] \ , \quad (9)$$

where Z_{eff} is the effective ion charge, n_i is the ion concentration, the quantities $k_B T_e$ and hc/λ are in eV, $\exp[-hc/(\lambda\, k_B T_e)] \approx 1$ and $\tilde{g}_{ff}$ is the so-called Gaunt factor that depends weakly on T_e and the radiation wavelength λ, and accounts for the quantum effects, the electron screening of nuclei, etc.[10] Among the variety of expressions and values obtained and recommended for $\tilde{g}_{ff}$ of different types of plasma, we shall accept here (combining a recent suggestion[11,12] and a former result[10]) that

$$\tilde{g}_{ff}(\lambda, T_e) = \ln\left(\frac{k_B T_e}{(13.6h^2c^2/\lambda^2)^{1/3}}\right)^{0.827} \ , \quad (10)$$

where $k_B T_e$ and hc/λ are in eV again. On the basis of Eqs.(9) and (10), assuming that $n_i = n_e$ and $Z_{\text{eff}} = 1$, for the photon counting rate spectrum of the bremsstrahlung-due parasitic signal $N_{br}(\lambda_s)$ interfering with the useful signal $N[\lambda_s; t(z)]$, we obtain

$$N_{br}(\lambda_s) = 6.25\times10^{-21}[K(\lambda_i,\lambda_s)/K_t(\lambda_i)]A_D\Delta\Omega_D\lambda_s^{-1}\int dz \ln\left[k_B T_e(z)/(13.6h^2c^2/\lambda_s^2)^{1/3}\right] n_e^2(z)[k_B T_e(z)]^{-1/2} \ , \quad (11)$$

where A_D is the photon detector effective area, $\Delta\Omega_D$ is the solid angle determined by the relative aperture of the receiving optics, and the product $A_D\Delta\Omega_D$ is the so-called etendue. For a spectral interval $[\lambda_{s1},\lambda_{s2}]$ we have

$$N_{br}(\lambda_{s1},\lambda_{s2}) = 6.25\times10^{-21} A_D \Delta\Omega_D \int dz n_e^2(z)[k_B T_e(z)]^{-1/2} \int_{\lambda_{s1}}^{\lambda_{s2}} d\lambda_s [K(\lambda_i,\lambda_s)/K_t(\lambda_i)]\lambda_s^{-1} \ln\left[k_B T_e(z)/(13.6h^2c^2/\lambda_s^2)^{1/3}\right] =$$

$$= 6.25\times10^{-21} A_D \Delta\Omega_D [K(\lambda_i,\overline{\lambda}_s)/K_t(\lambda_i)] \ln(\lambda_{s2}/\lambda_{s1}) \int dz n_e^2(z)[k_B T_e(z)]^{-1/2} \ln\left[k_B T_e(z)/(13.6h^2c^2/\overline{\lambda}_s^2)^{1/3}\right] \quad , \quad (12)$$

where $\overline{\lambda}_s \in [\lambda_{s1},\lambda_{s2}]$.

2.3 Noise effects

The noise accompanying the lidar return signal may consist of various components. Let us first consider the photon counting mode of detection where the photon counts (single photoelectron pulses) registered during a time interval T are in fact the signal. In this case the signal itself undergoes Poisson fluctuations whose variance $\mathrm{Var}\{N[\lambda_{s1},\lambda_{s2};t(z)]T\}$ is equal to the mean signal value, that is, to the mean number of photon counts $N[\lambda_{s1},\lambda_{s2};t(z)]T$ for the period T. Obviously, the signal-to-noise ratio $\mathrm{SNR}=[(NT)^2/\mathrm{Var}\{NT\}]^{1/2}$ is then equal to $(NT)^{1/2}$. The parasitic background interfering with the useful signal consists of plasma light photon counts and dark counts due to thermonic and autoelectronic emission. It also has Poisson statistics with mean value $N_b(\lambda_{s1},\lambda_{s2})T=[N_{br}(\lambda_{s1},\lambda_{s2})+N_{dc}]T$ and variance $\mathrm{Var}\{N_b(\lambda_{s1},\lambda_{s2})T\}=N_b(\lambda_{s1},\lambda_{s2})T$, where N_{dc} is the dark count rate. The background leads to adding $N_b(\lambda_{s1},\lambda_{s2})T$ to the mean value and to the variance of the measured signal. To eliminate the bias-up of the signal one should subtract from the measurement result an experimental estimate $\hat{N}_b(\lambda_{s1},\lambda_{s2})T$ of N_bT. Then the bias will be eliminated but a new fluctuation component will be added, with variance $\mathrm{Var}\{\hat{N}_b(\lambda_{s1},\lambda_{s2})T\}$. At a precise enough estimate $\hat{N}_bT$, based, e.g., on a measurement for a time interval exceeding essentially T, we shall have $\mathrm{Var}\{\hat{N}_bT\} << N_bT$. Then the overall measurement variance will remain equal to $N[\lambda_{s1},\lambda_{s2};t(z)]+N_b(\lambda_{s1},\lambda_{s2})$, and the signal-to-noise ratio will be

$$\mathrm{SNR}=(NT)^{1/2}/(1+N_b/N)^{1/2} \quad . \quad (13)$$

In practice, the single-photoelectron flux after the photocathode is amplified in a microchannel plate (MCP) photomultiplier tube (PMT) and is transformed into a signal current i (or voltage v)[13-15]. The process of amplifying leads to the arising of an additional noise (in excess of the Poisson noise) due to the fluctuations of the single-electron pulse shapes and charges. Then the ensemble-mean signal photocurrent (concerning say the useful signal) is $i[\lambda_{s1},\lambda_{s2};t(z)]=GN[\lambda_{s1},\lambda_{s2};t(z)]$, where G (somewhere called the gain[3]) should be interpreted as the mean single-(photo)electron-induced charge through the PMT circuit. The corresponding photocurrent variance is $\mathrm{Var}\{i\}=F_eG^2N/\theta$, where $\theta=\tau_{de}$ is the photon detector response time, and F_e is an excess-noise factor accounting for the noise enhancement[3,14]. Then the signal-to-noise ratio $\mathrm{SNR}=i/\mathrm{Var}\{i\}^{1/2}=(N\theta/F_e)^{1/2}$. In an analogous way one may obtain that the variance of the background current $i_b=GN_b(\lambda_{s1},\lambda_{s2})$ is $\mathrm{Var}\{i_b\}=F_eG^2N_b/\theta$, and the overall measurement signal-to-noise ratio is $\mathrm{SNR}=i/(\mathrm{Var}\{i\}+\mathrm{Var}\{i_b\})^{1/2}=(N\theta/F_e)^{1/2}/(1+N_b/N)^{1/2}$.

The PMT output is finally digitized and thus represented in a digital code describing, e.g., an average current over the digitizing step T_d. Certainly the measurement procedure is implied to include the above-discussed subtraction of an accurate estimate of the background (here, of i_b). Then, if $T_d<\theta$ the same as above expression for SNR is valid in practice. In the opposite case, when $\theta<T_d$, the same expression for SNR is obtained again, but with T_d instead of θ [13]. Otherwise, one may write that

$$\mathrm{SNR}=[N\max(\theta,T_d)/F_e]^{1/2}/(1+N_b/N)^{1/2} \quad . \quad (14)$$

The comparison of Eq.(14) and Eq.(13) suggests that the real measurement procedure is equivalent to a photon counting signal detection with F_e-times lower quantum efficiency and measurement interval $T=\max(\theta,T_d)$. This analogy is physically and experimentally substantiated in Ref.16. It is valid as well when measuring only the useful signal without background ($N_b=0$), or only the background in the absence of signal (see above the expressions of i_b and $\mathrm{Var}\{i_b\}$). The estimate $T=\max(\theta,T_d)$ of the effective photon counting interval (conditioning the measurement SNR) is physically interpretable by that the longer of both the time scales θ and T_d determines in fact the (better) averaging (spectrum narrowing) of the signal fluctuations[13]. Usually $\theta>T_d$ in the contemporary photon detection devices of interest[3,14,15]. The indicated analogy is especially useful for computer simulations and error analysis[11,14-16]. Note meanwhile that digitizing is also a source of noise that could be minimized to a negligible value by a proper choice of the digitizer scale.

3. ERRORS IN THE DETERMINATION BY DIFFERENT APPROACHES OF THE ELECTRON TEMPERATURE IN THERMONUCLEAR PLASMA

In this Section we shall consider single-shot TS lidar measurement of T_e in fusion plasma at a fixed LOS point z_0.

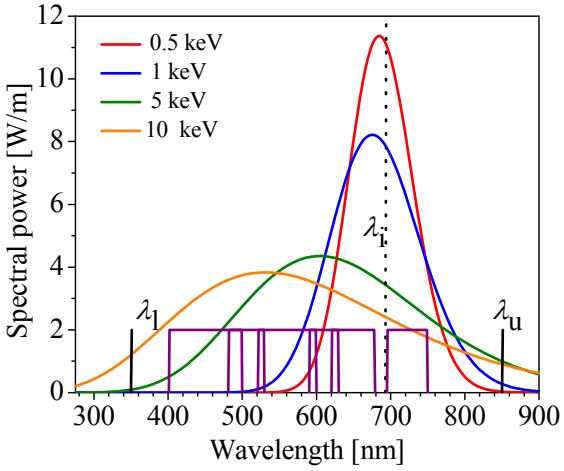

Fig. 1. Thomson backscattering spectrum for different electron temperatures at a sensing radiation wavelength λ_i=694 nm. The working spectral interval employed is $[\lambda_l,\lambda_u]$ with λ_l=350 nm and λ_u=850 nm. The spectral subintervals used in the "center-of-mass wavelength" and fitting approaches are also shown.

3.1 Linear error propagation

Let us consider M spectral intervals $[\lambda_{s1k},\lambda_{s2k}]$ (k=1,...M) from the relativistic Thomson backscattering spectrum from fusion plasma (see Fig.1), which are selected by the receiving optical system of the lidar. The mean detected signals in the corresponding measurement channels may be denoted as $i_k = i[\lambda_{s1k},\lambda_{s2k};t(z_0);n_e,T_e]=i_k(T_e)$, where n_e and T_e are respectively the electron concentration and temperature at $z=z_0$. We shall further assume that T_e may vary at a constant value of n_e. Suppose as well that some composition of i_k exists,

$$C(i_1, i_2,\ldots, i_M)=f(T_e) \ , \tag{15}$$

that is unambiguous function, $f(T_e)$, of the electron temperature. Then, the temperature T_e is expressible by the inverse function

$$T_e = f^{-1}(C) = \varphi\,[C(i_1, i_2,\ldots, i_M)] \ . \tag{16}$$

The measurement process provides in practice some estimates (statistical realizations) $\hat{i}_k$ of the signals i_k. The corresponding estimate $\hat{T}_e$ of T_e is given in this case as

$$\hat{T}_e = \varphi[C(\hat{i}_1,\hat{i}_2,...,\hat{i}_M)] \ . \tag{17}$$

At relatively small fluctuations of $\hat{i}_k$ around i_k (at large enough SNR>>1) they may be considered as differential quantities $di_k = \hat{i}_k - i_k$. This allows one, by using Taylor series expansion, to represent $\hat{T}_e$ in the form

$$\hat{T}_e = T_e + (d\varphi/dC)\sum_{k=1}^{M}(\partial C/\partial i_k)di_k + \frac{1}{2}\left\{(d^2\varphi/dC^2)\left[\sum_{k=1}^{M}(\partial C/\partial i_k)di_k\right]^2 + (d\varphi/dC)\sum_{k,l=1}^{M}\frac{\partial^2 C}{\partial i_k \partial i_l}di_k di_l\right\} + \ldots \ , \tag{18}$$

where $d\varphi/dC = 1/f'(T_e)$, and $d^2\varphi/dC^2 = -f''(T_e)/[f'(T_e)]^3$. An estimate of the rms error δT_e in the determination of T_e is obtainable from Eq.(18) as

$$\delta T_e = \left\langle (\hat{T}_e - T_e)^2 \right\rangle^{1/2} = |\partial\varphi/\partial C|\left\{\sum_{k=1}^{M}(\partial C/\partial i_k)^2 \mathrm{Var}\{i_k\}\right\}^{1/2} \ , \tag{19}$$

where the signals i_k and i_l for $l \neq k$ are naturally supposed to be statistically independent of each other, and $\langle . \rangle$ denotes ensemble average. Also, an estimate of the statistical bias $\delta_b T_e$ may be obtained as

$$\delta_b T_e = \left\langle \hat{T}_e - T_e \right\rangle = \frac{1}{2} \frac{d^2\varphi / dC^2}{(d\varphi / dC)^2} (\delta T_e)^2 + (d\varphi / dC) \sum_{k=1}^{M} \frac{\partial^2 C}{\partial i_k^2} \mathrm{Var}\{i_k\} \ . \tag{20}$$

Let us preliminary note that in the concrete results obtained below for δT_e and $\delta_b T_e$, we shall have taken into account the relations (see Sec.2.3) $i_k = GN_k$ and $\mathrm{Var}\{i_k\}=(F_e G^2/T)(N_k+N_{bk})$, where N_k and N_{bk} are respectively the signal and the background photocathode counting rates in the kth channel, and $T=\max(\theta,T_d)$.

3.2 Approach based on the temperature dependence of the ratio of the signals from two spectral intervals

Consider now two spectral intervals of the relativistic Thomson backscattering spectrum, $[\lambda_{s11},\lambda_{s21}]$ and $[\lambda_{s12},\lambda_{s22}]$ (k=1 and 2, respectively). According to Eq.(6), the ratio C of the signals i_1 and i_2 is given as

$$C = i_1 / i_2 = \int_{\lambda_{s11}}^{\lambda_{s21}} K_n(\lambda_i, \lambda_s) \eta(\lambda_s, z) \xi_2(\lambda_i, \lambda_s, v_{th}) d\lambda_s \Big/ \int_{\lambda_{s12}}^{\lambda_{s22}} K_n(\lambda_i, \lambda_s) \eta(\lambda_s, z) \xi_2(\lambda_i, \lambda_s, v_{th}) d\lambda_s \ . \tag{21}$$

This ratio is unambiguous function,

$$C = f(T_e) \ , \tag{22}$$

of the electron temperature T_e and may be used for measuring it.

The rms error estimate δT_e in the determination of the electron temperature T_e, obtained by linear error transfer, is given by the following expression

$$\delta T_e = \left| d \ln f(T_e) / dT_e \right|^{-1} \left\{ F_e \sum_{k=1}^{2} (N_k T)^{-1} (1 + N_{bk} / N_k) \right\}^{1/2} \ . \tag{23}$$

So it is clear that the measurement accuracy is naturally proportional to the measurement sensitivity $\left| d \ln f(T_e) / dT_e \right|$ and the mean signal intensities ($\propto N_1$ and N_2). The corresponding statistical bias is

$$\delta_b T_e = [d \ln f(T_e) / dT_e]^{-1} F_e (N_2 T)^{-1} (1 + N_{b2} / N_2) - (1/2)\left[f''(T_e) / f'(T_e) \right] (\delta T_e)^2 \ . \tag{24}$$

3.3 Approach based on the temperature dependence of the "center-of-mass wavelength" of the relativistic Thomson spectrum

Let us consider again M spectral intervals $(\lambda_{s1k},\lambda_{s2k})$, k=1,...,M. The central wavelength of the kth interval is $\lambda_k = (\lambda_{s1k}+\lambda_{s2k})/2$. Then the center-of-mass wavelength λ is defined as

$$\lambda = \left(\sum_k \lambda_k i_k \right) \Big/ \left(\sum_k i_k \right) = \left(\sum_k \lambda_k N_k \right) \Big/ \left(\sum_k N_k \right) = f(T_e) \ , \tag{25}$$

where $f(T_e)$ is unambiguous function of the electron temperature (see also Fig.1). An explicit writing of Eq.(25) is

$$\lambda = \sum_k \lambda_k \int_{\lambda_{s1k}}^{\lambda_{s2k}} K_n(\lambda_i, \lambda_s) \eta(\lambda_s, z) \xi_2(\lambda_i, \lambda_s, v_{th}) d\lambda_s \Big/ \sum_k \int_{\lambda_{s1k}}^{\lambda_{s2k}} K_n(\lambda_i, \lambda_s) \eta(\lambda_s, z) \xi_2(\lambda_i, \lambda_s, v_{th}) d\lambda_s \ . \tag{26}$$

The linear error propagation approach leads in this case to the following expression of the rms error δT_e in the determination of T_e on the basis of the dependence $\lambda = f(T_e)$:

$$\delta T_e = \left| d \ln f(T_e) / dT_e \right|^{-1} \left(\sum_k N_k T \right)^{-1} \left\{ F_e \sum_{k=1} \left(\frac{\lambda_k - \lambda}{\lambda} \right)^2 N_k T (1 + N_{bk} / N_k) \right\}^{1/2} \ . \tag{27}$$

The corresponding expression of the statistical bias is

$$\delta_b T_{\rm e} = [d \ln f(T_{\rm e})/dT_{\rm e}]^{-1}\left(\sum_k N_k T\right)^{-2} F_{\rm e}\sum_{k=1}\left(\frac{\lambda_k-\lambda}{\lambda}\right)^2 N_k T(1+N_{\rm bk}/N_k) - (1/2)\left[f''(T_{\rm e})/f'(T_{\rm e})\right](\delta T_{\rm e})^2 . \quad (28)$$

3.4 Approach based on fitting the data to the temperature-dependent relativistic Thomson spectrum

3.4.1 Log-linear fit

In this case, following Mattioli and Papoular[17], we obtain that (when $T_{\rm e}$ is in eV)

$$\delta T_e = 4\times 10^{-6} T_e^2 \sigma_b \quad , \quad (29)$$

where $b = -(c/v_{th})^2$ is one of the parameters to be determined by fitting,

$$\sigma_b = \left(\frac{\sum_{k=1}^{M}{\rm SNR}_k^2}{\left(\sum_{k=1}^{M}{\rm SNR}_k^2\right)\left(\sum_{k=1}^{M}{\rm SNR}_k^2 Z_k^2\right)-\left(\sum_{k=1}^{M}{\rm SNR}_k^2 Z_k\right)^2}\right)^{1/2} \quad (30)$$

is the rms error in the determination of b, ${\rm SNR}_k^2 = N_k T/[F_e(1+N_{bk}/N_k)]$, N_k is estimated by using Eq.(3), and

$$Z_k = (\lambda_i/\lambda_k)^{1/2} + (\lambda_k/\lambda_i)^{1/2} - 2 \ . \quad (31)$$

The statistical bias is obtained in the form

$$\delta_b T_e = \frac{(\delta T_e)^2}{T_e} + 1.97\times 10^{-6} T_e^2\left(M\sum_{k=1}^{M} Z_k {\rm SNR}_k^2 - \sum_{k=1}^{M} Z_k \sum_{k=1}^{M}{\rm SNR}_k^2\right)\Big/\left[\left(\sum_{k=1}^{M}{\rm SNR}_k^2\right)\sum_{k=1}^{M} Z_k^2{\rm SNR}_k^2 - \left(\sum_{k=1}^{M} Z_k{\rm SNR}_k^2\right)^2\right] \quad (32)$$

3.4.1 Non-linear fit

In this case we consider $a = n_{\rm e}\left(1+\frac{15}{16}\frac{1}{b^2}+\frac{105}{512}\frac{1}{b^4}\right)^{-1}$ and $b=c/v_{\rm th}$ as two parameters to be determined by fitting. Then, following the common procedure of non-linear least-squares fitting[18] of the experimental data to the theoretical TS spectrum, we obtain two transcendental in general equations with respect to a and b. One of these equations is linear with respect to a and allows one to express it (a) through b and the experimental data $\hat{i}_k$. By replacing the expression obtained for a in the second equation, we obtain a relation between b and $\hat{i}_k$. On the basis of this relation we further obtain another one, between the differential db of b (and respectively d$T_{\rm e}$ of $T_{\rm e}$) and the differentials di_k of $\hat{i}_k$. At last, by averaging $({\rm d}T_{\rm e})^2$ we obtain an estimate of $\delta T_{\rm e} = <({\rm d}T_{\rm e})^2>^{1/2}$ depending on Var$\{i_k\}$ and i_k. What is interesting to note here is that the result we have obtained for $\delta T_{\rm e}$, after cumbersome derivations, coincides absolutely with the one obtained in the log-linear case. That is, $\delta T_{\rm e}$ is given again by Eqs.(29) and (30). By using the same implicit differentiation approach, the bias is estimated as $\delta_b T_{\rm e} = \frac{1}{2}\sum_k \frac{\partial^2 T_e}{\partial i_k^2}{\rm Var}\{i_k\}$. The result obtained is given by a formula like Eq.(32) where the factor $\left(M\sum_{k=1}^{M} Z_k{\rm SNR}_k^2 - \sum_{k=1}^{M} Z_k\sum_{k=1}^{M}{\rm SNR}_k^2\right)$ alone is replaced by another one, $\left(2\sum_{k=1}^{M} Z_k{\rm SNR}_k^2 - \sum_{k=1}^{M}{\rm SNR}_k^2 D_n/D\right)$;

$D_n = \sum_{k=1}^{M}{\rm SNR}_k^2\sum_{k=1}^{M} Z_k^3{\rm SNR}_k^2 - \sum_{k=1}^{M} Z_k{\rm SNR}_k^2\sum_{k=1}^{M} Z_k^2{\rm SNR}_k^2$, and $D = \sum_{k=1}^{M}{\rm SNR}_k^2\sum_{k=1}^{M} Z_k^2{\rm SNR}_k^2 - \left(\sum_{k=1}^{M} Z_k{\rm SNR}_k^2\right)^2$.

4. SIMULATIONS AND NUMERICAL ANALYSIS

The simulations and the analysis performed below will be based on the analogy commented in Sec.2.3, between the real measurement procedure and a photon detection with measurement interval $T=\max(\theta,T_d)$ and F_e – times lower photocathode quantum efficiency compared to the true one, K_q. In other words, the photon counts NT, due to the useful signal, and the background photon counts $N_bT=N_{br}T$, will be evaluated using Eqs.(4) and (12), respectively, where K_q is replaced by the so-called effective quantum efficiency $EQE=K_q/F_e$ [11,14,15]. The dark counts will not be especially considered.

The fusion plasma will be supposed to occupy the LOS region between z=7 m and z=9 m. It will be supposed as well that z_0=8 m. The longitudinal (LOS) distributions of the electron temperature and concentration will be considered as uniform. Furthermore, the temperature will be varied (from T_e=0.1 keV to T_e=10 keV with a step ΔT_e=0.1 keV) at a constant value of $n_e=3.10^{19}$ m^{-3}. The receiving aperture (receiving mirror) diameter D_m and the etendue $E=A_D\,\Delta\Omega_D$ of the receiving optics are assumed to be respectively D_m=0.7 m and E=4 cm^{2}sr. The sensing laser radiation is supposed to have wavelength λ_i=694 nm and to enter the active zone through a penetration aperture with longitudinal coordinate z_p=7 m and diameter D_p=0.26 m. The sensing laser pulse-beam will be assumed to have energy E_0=0.6 J, duration τ_p=300 ps, and diameter D_l=0.07 m. Under the above-described conditions the penetration aperture will not affect the process of collection of the backscattered radiation. That is, the vignetting factor in this case will be equal to unity. Unlike that, the vignetting will essentially reduce the plasma light background. In principle, in the latter case the vignetting factor, F_v, could be evaluated. Nevertheless, it is more expedient to be determined by suitable calibration. According to some preliminary estimates we have made and to some available data[11], the vignetting factor may be taken to be F_v=0.33. We shall also assume that the optical background is additionally lowered two times (e.g.[6]) by using polarizer for selecting only the polarization component of the lidar return that is parallel to the polarization of the sensing radiation. The effective photon counting interval $T=\max(\theta,T_d)$ will be accepted to have a duration of 250 ps.

In accordance with the spectral sensitivity ranges of the available photon detectors[14], we shall suppose observing the TS spectrum within the wavelength region from λ_l=350 nm to λ_u=850 nm. For applying the first of the concerned here T_e–measurement methods, the wavelength interval $[\lambda_l,\lambda_u]$ should be divided into two subintervals $[\lambda_{s11},\lambda_{s21}]$ and $[\lambda_{s12},\lambda_{s22}]$, where $\lambda_{s21}=\lambda_{s12}=\lambda_m$. For applying the center-of-mass approach or the fitting approach, the interval $[\lambda_l,\lambda_u]$ should be divided into several subintervals. Further, we assume that $K_t(\lambda_i)$=0.75, $K_t(\lambda_s)$=0.25 for $\lambda_s\in[\lambda_l,\lambda_u]$, $K_f(\lambda_s)$=1, and $K_q(\lambda_s)/F_e=EQE$=0.05 for all the measurement channels (about such a possibility one could see, e.g., in [14]). Finally, because of the weak spectral dependence of the Gaunt factor, the evaluation of the photon counting rate of the bremsstrahlung will be simplified by setting $\overline{\lambda}_s=\lambda_i$ in Eq.(12).

The described above characteristic parameters are chosen to be as close as possible to those of the JET TS lidar system.

4.1 Estimation by Monte-Carlo simulations of the error in the determination of T_e by the new approaches

4.1.1 Ratio of the signals from two spectral regions

In this case we consider the above-described pairs of spectral intervals $[\lambda_l,\lambda_m]$ and $[\lambda_m,\lambda_u]$. For each value of T_e the corresponding mean TS photon count rates are evaluated on the basis of Eq.(4). They may be denoted by $N_1(T_e)$ and $N_2(T_e)$. The corresponding mean bremsstrahlung photon count rates, $N_{br1}(T_e)$ and $N_{br2}(T_e)$ are evaluated on the basis of Eq.(12) with $\overline{\lambda}_s=\lambda_i$, taking into account the vignetting and polarization effects. Then on the basis of the results obtained, the functions

$$f(T_e)=N_1(T_e)/N_2(T_e) \tag{33}$$

are determined (Fig.2) as well as the corresponding temperature-dependent errors and biases, $\delta T_e(T_e)$ and $\delta_b T_e(T_e)$.

The Monte-Carlo simulations are performed in the following way. At known mean values $N_1(T_e)T$ and $N_2(T_e)T$, and $N_{br1}(T_e)T$ and $N_{br2}(T_e)T$, by using Poisson random-number generator we produce H=100 realizations, $\hat{N}_1^l(T_e)T$, $\hat{N}_2^l(T_e)T$, $\hat{N}_{br1}^l(T_e)T$ and $\hat{N}_{br2}^l(T_e)T$, of the photon counts of the useful signal and the background; l=1,2,…,100. Then we compose the quantities $\hat{N}_1^lT+\hat{N}_{br1}^lT-N_{br1}T$ and $\hat{N}_2^lT+\hat{N}_{br2}^lT-N_{br2}T$.

Next, by using the reference functions $f(T_e)$ and the ratios $(\hat{N}_1^l T + \hat{N}_{br1}^l T - N_{br1} T)/(\hat{N}_2^l T + \hat{N}_{br2}^l T - N_{br2} T)$ we obtain hundred estimates $\hat{T}_e^l$ of the electron temperature. Then, an estimate $\hat{\delta}T_e$ of the rms error δT_e will be

$$\hat{\delta}T_e = \left[H^{-1} \sum_{l=1}^{H} (\hat{T}_e^l - T_e)^2 \right]^{1/2} . \tag{34}$$

In Fig.3 we have compared a Monte-Carlo estimate $\hat{\delta}_r T_e(T_e) = \hat{\delta}T_e(T_e)/T_e$, of the relative error in the determination of the electron temperature, with the theoretical estimate $\delta_r T_e(T_e) = \delta T_e(T_e)/T_e$ obtained by Eq.(23). It is seen that both the results are consistent. One may notice as well that lowering the value of λ_m leads to increasing $\delta_r T_e$, for $T_e < 1$ keV, and to decreasing it, for $T_e > 1$ keV. At the same temperatures ($T_e > 1$ keV) the bias is evaluated to be two orders of magnitude lower than the rms error.

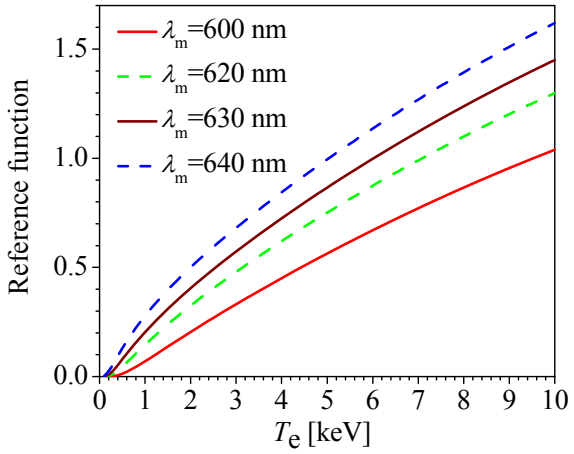

Fig. 2. Reference functions $f(T_e)$ [Eq.(33)] in the case of using the ratio of the signals from two spectral intervals.

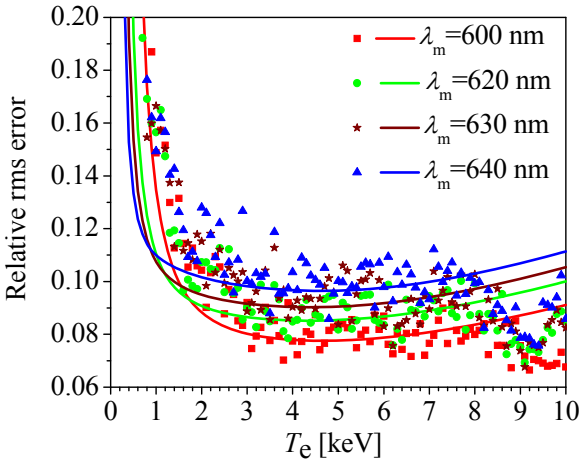

Fig. 3. Relative rms error $\delta T_e/T_e$ in the determination of the electron temperature T_e, vs T_e, in the case of using the ratio of the signals from two spectral intervals. The theoretical results and the results from Monte-Carlo simulations are represented respectively by curves and points.

4.1.2 Center-of-mass wavelength approach

In this case M spectral subintervals $\Delta_k=[\lambda_{s1k},\lambda_{s2k}]$ are employed (Fig.1). The mean TS and background photon count rates $N_k(T_e)$ and $N_{brk}(T_e)$ are evaluated by using Eqs.(4) and (12), respectively. Then, according to Eq.(25), the reference function $\lambda(T_e)=f(T_e)$ is built (Fig.4). The knowledge of $N_k(T_e)$ and $N_{brk}(T_e)$ allows one to determine, by using Eqs.(27) and (28), the temperature-dependent relative errors and biases $\delta_r T_e(T_e)$ and $\delta_b T_e(T_e)$. The results $\delta_r T_e(T_e)$obtained for six optimum "JET subintervals" are shown in Fig.5.

The simulations are performed as in the preceding section. That is, at known mean values $N_k(T_e)T$ and $N_{brk}(T_e)T$, by Poisson random-number generator we produce H=100 realizations $\hat{N}_k^l(T_e)T$ and $\hat{N}_{brk}^l(T_e)T$ of the useful-signal and the background photon counts; l=1,2,…,100. Afterwards we compose the quantities $\hat{N}_k^l(T_e)T + \hat{N}_{brk}^l(T_e)T - N_{brk}(T_e)T$ to use them, together with the reference function $f(T_e)$, for obtaining hundred estimates $\hat{T}_e^l$ of the electron temperature. Certainly, an estimate $\hat{\delta}T_e$ of the measurement error δT_e is given again by Eq.(34). A Monte-Carlo estimate $\hat{\delta}T_e(T_e)$ is compared in Fig.5 with the theoretical estimate obtained by Eq.(27). It is seen that the result from the simulations is in accordance with the theoretical result. The estimation of the bias $\delta_b T_e$ shows that for $T_e > 1$ keV, for both the center-of-mass and the fitting approaches, it is again two orders of magnitude lower than the rms error δT_e.

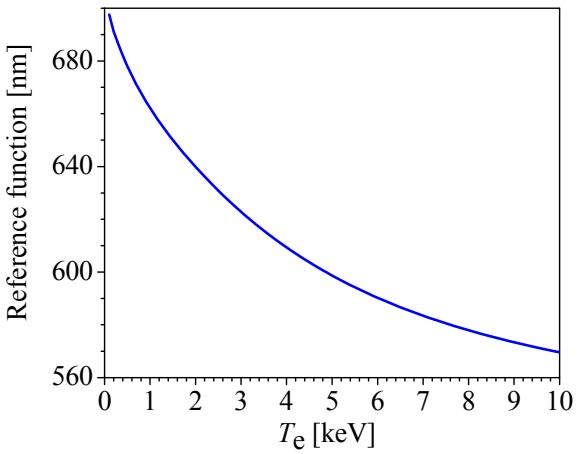

Fig. 4. Reference function $\lambda=f(T_e)$ when using the center-of-mass wavelength approach with six optimum JET subintervals shown in Fig.1.

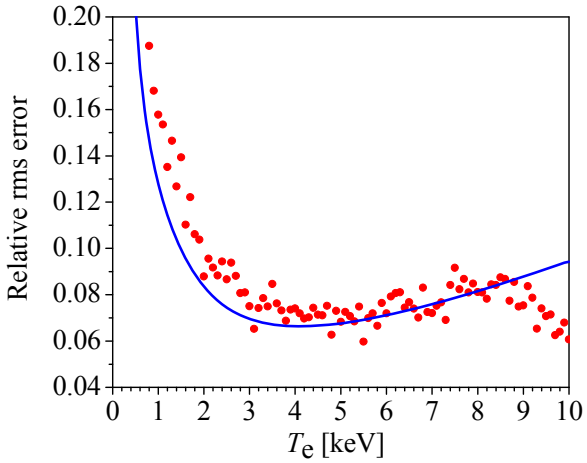

Fig. 5. Relative rms error $\delta T_e/T_e$ in the determination of the electron temperature T_e, vs T_e, when using the center-of-mass wavelength approach with six JET spectral channels. The theoretical results and the results from Monte-Carlo simulations are represented respectively by curve and circles.

4.2 Potential accuracies of the different approaches for measuring T_e

The relative rms error $\delta_r T_e=\delta T_e/T_e$ may be considered as a reciprocal characteristic of the potential accuracy (potential efficiency) of a method for measuring T_e. Therefore, to compare the efficiencies of the three T_e-measurement approaches under consideration here, we have compared graphically in Fig.6 the corresponding relative errors $\delta_r T_e(T_e)=\delta T_e(T_e)/T_e$. For calculation of the errors we have used Eqs.(23), (27), and (30). The fitting approach is assumed to employ the same number and allocation of the spectral intervals Δ_k as the center-of-mass wavelength approach. The experimental conditions and characteristic parameters supposed are described in detail above. It is seen in the Figure that for T_e>1 keV the three approaches have practically the same efficiency with a slight advantage of the fitting approach. Note as well that the "ratio-of-powers" approach is considered to use the whole spectral region $[\lambda_l,\lambda_u]$; its efficiency will naturally decrease with narrowing the spectral subintervals employed. For T_e<1 keV the novel approaches have lower efficiency because of lower T_e -measurement sensitivity.

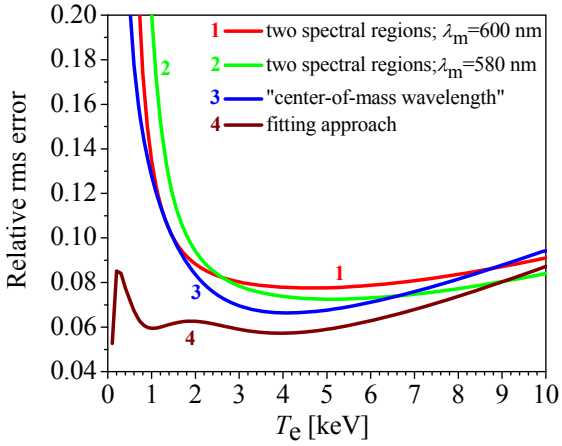

Fig. 6. Theoretically estimated relative rms errors $\delta T_e/T_e$, vs T_e, in the determination of the electron temperature T_e by using the ratio of the signals from two spectral intervals, λ_m=600 nm (1) and λ_m=580 nm (2); the center-of-mass wavelength (3), and the fitting approach (4). Curves (3) and (4) are evaluated assuming the use of the six optimum JET channels.

5. CONCLUSION

In the present work we have proposed and estimated analytically and by simulations the potential accuracy (efficiency) of two novel approaches to measuring by TS lidar the electron temperature in thermonuclear plasmas. The approaches proposed are based on an analysis of the relativistic TS spectrum. One of them is based on the unambiguous temperature dependence of the ratio of the return-signal powers of two spectral regions. The second approach is based on the unambiguous temperature dependence of the "center-of-mass wavelength" of the lidar-return spectrum. The potential efficiency is characterized in fact by the temperature-dependent rms relative error in the determination of the electron temperature. Therefore, we have first derived analytical expressions of the corresponding temperature-measurement rms errors. The validity of the expressions derived is confirmed by Monte-Carlo simulations. We have considered as main sources of measurement uncertainties (noise) the bremsstrahlung-due plasma light background and the enhanced (in MCP PMT) photon-counting Poisson fluctuations. The comparison, under uniform experimental conditions, of the (log-linear or non-linear) fitting approach with the novel approaches shows that at T_e>1 keV the latter ones (at slightly larger rms error) may practically achieve the same efficiency as the fitting approach. Thus, the three approaches can be used for mutually validating the results obtained for the electron temperature. They may be used as well for distinguishing the real inhomogeneities in the recovered T_e profiles from seeming ones due to statistical fluctuations. Practical advantages of the new approaches may be the simple, clear and stable measurement procedures without any additional hypothesis or considerations about the weight or the variance of the experimental data or the goodness of the fit. Note as well that the new approaches as well as the fitting approach lead to practically unbiased estimates of T_e.

It is useful to mention as well some additional conclusions resulting from the investigations performed. First, the effective measurement interval of the equivalent photon-counting signal detection is equal to the larger of the digitizing step and the response time of the photon detector. In practice, the larger and determinant quantity is the photodetector response time. And second, the linear error propagation estimates of the rms errors in the determination of the electron temperature by log-linear or non-linear fitting are given by the same expression.

Further efforts, in the field concerned here, should be directed to investigating the distortion effect of a relatively long (with respect to the fusion plasma variation scales) lidar pulse response on the profiles of the electron temperature and concentration. It is also important and useful to see how could any deconvolution procedure help in this case.

ACKNOWLEDGEMENTS

The investigations described in the work have been supported by the EURATOM/INRNE Fusion Association and partially by the Bulgarian National Science Fund under the project F-1511. The authors are grateful to Dr. Mike Walsh and Dr. Marc Beurskens (EURATOM/UKAEA Fusion Association, Culham Science Centre, UK) for the rich information and experience shared and for the stimulating discussions on different problems concerned in the work.

APPENDIX A

In order to reduce the effects of the stray light and the plasma light background, one usually selects by polarizer and measures only the polarization component of the TS lidar return that is parallel to the polarization of the incident (sensing) laser radiation. Taking into account the relativistic depolarization effects on the (back)scattered radiation, Naito et al. have derived a practically exact analytical expression of the TS spectrum. In the case of backscattering (at angle π) this expression may be written, e.g., in the form (see also [1,2]),

$$\beta_{\text{Naito}}[\lambda_i;\lambda_s;\, n_e(z),T_e(z)] = \beta_{\text{Mattioli}}[\lambda_i;\lambda_s;\, n_e(z),T_e(z)][1+\delta(q)]\ , \tag{A1}$$

where the expression of $\beta_{\text{Mattioli}}[\lambda_i;\lambda_s;\, n_e(z),T_e(z)]$ is given by Eq.(5),

$$\delta(q) = \{\beta_{\text{Naito}}[\lambda_i;\lambda_s;\, n_e(z),T_e(z)] - \beta_{\text{Mattioli}}[\lambda_i;\lambda_s;\, n_e(z),T_e(z)]\} \,/\, \beta_{\text{Mattioli}}[\lambda_i;\lambda_s;\, n_e(z),T_e(z)] \tag{A2}$$

is the relative difference between the spectral distributions of Naito and Mattioli,

$$\delta(q) = 2e^q\left[E_3(q) - 3E_5(q)\right] = \frac{1}{2}\left\{\frac{q^3}{2} - \frac{q^2}{2} - q - 1\right\} + q^2\left(1 - \frac{q^2}{4}\right)e^q E_1(q)\ , \tag{A3}$$

$E_n(q) = \int_1^\infty \frac{e^{-qx}}{x^n} dx$ is the exponential integral of the nth order, and $q = \frac{m_e c^2}{2k_B T_e}\left(\sqrt{\lambda_s / \lambda_i} + \sqrt{\lambda_i / \lambda_s}\right)$. The dependence of $\delta(q)$ on T_e for $\lambda_s = \lambda_i$ is represented in Fig.A1.

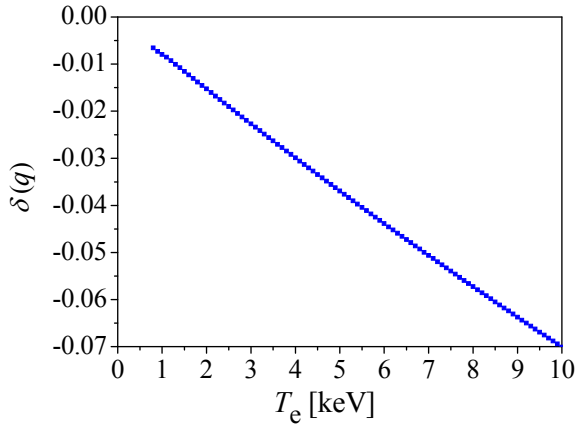

Fig. A1. Temperature dependence of the relative difference between the spectral distributions of Naito and Mattioli.

REFERENCES

[1] Mattioli, M., "Incoherent light scattering from high temperature plasmas," EUR-CEA-FC-752 (1974)

[2] Naito, O., Yoshida, H. and Matoba, T., "Analytic formula for fully relativistic Thomson scattering spectrum," Phys. Fluids B5(11), 4256-4258 (1993).

[3] Kampenaars, M. et al., "Comparison of multialkali and GaAs photocathode detectors for Joint European Torus edge light detection and ranging Thomson scattering profiles," Rev. Sci. Instrum. 75(10), 3894-3896 (2004).

[4] Walsh, M. et al., "Design challenges and analysis of the ITER core LIDAR Thomson scattering system," Rev. Sci. Instrum. 77, 10E525 (2006).

[5] Griem, H., [Plasma Spectroscopy], McGrawHill, New York (1964).

[6] Sheffield, J., [Plasma Scattering of Electromagnetic Radiation], Academic, New York, 191–210 (1975).

[7] Hutchinson, I. H., [Principles of Plasma Diagnostics], Cambridge University Press, Cambridge (1987).

[8] Bekefi, G., [Radiation Processes in Plasmas], Wiley, New York (1966).

[9] Foord, M. E., Marmar, E. S. and Terry, J. L., "Multichannel light detector system for visible continuum measurements on Alcator C," Rev. Sci. Instrum. 53(9), 1407-1409 (1982).

[10] Brussaard, P. J., Van de Hulst, H. C., "Approximation formulas for nonrelativistic bremsstrahlung and average Gaunt factors for a Maxwellian electron gas," Rev. Mod. Phys. 34(3), 507-520 (1962).

[11] Beurskens, M., Guidicotti, L., Kempenaars, M., Scannel, R. and Walsh, M., "ITER Lidar performance analysis", 17th Topical Conference on High Temperature Plasma Diagnostics, Paper F31, May 11-15,2008, New Mexico, USA

[12] Walsh, M. and Morgan, P. (private information).

[13] Rytov, S.M., [Introduction to Statistical radiophysics], vol. I – Random processes, Nauka, Moskow (1976).

[14] Pasqualotto, R. and Nielsen, P. "GaAs photomultiplier for LIDAR Thomson scattering," Rev. Sci. Instrum. 74(3), 1671-1674 (2003).

[15] Pasqualotto, R. et al., "High resolution Thomson scattering for Joint European Torus (JET)," Rev. Sci. Instrum. 75(10), 3891-3893 (2004).

[16] Salzmann, H. et al., "The LIDAR Thomson scattering diagnostic on JET," JET-R(89) 07.

[17] Mattioli, M. and Papoular, R., "Analysis of light scattering data from relativistic plasmas," Plasma Physics 17, 165-172 (1975)

[18] Bevington, P. R. and Robinson, D. K. [Data Reduction and Error Analysis for the Physical Sciences], 2nd ed., McGraw–Hill, New York (1992).